Calculating Electromagnetic Force Created by Static Suspension Device Used in Permanent Magnet Electrodynamic Suspension Vehicle

Wenlong Zhang [1], Kunlun Zhang [1], Yin Chen [2], and Xijun Liu [3]

[1] Key Laboratory of Magnetic Suspension Technology and Maglev Vehicle Ministry of Education
Southwest Jiaotong University, Chengdu, 610031, China
zhangwenlong2010@outlook.com, zhangkunlun@263.net

[2] Electric Design and Research Institute
China Railway Eryuan Engineering Group Co., Ltd., Chengdu, 610031, China
chenyin_swjtu@126.com

[3]Aviation Engineering Institute
Civil Aviation Flight University of China, Guanghan, 618307, China
edwiin85617@163.com

Abstract ─ In response to the shortcomings of existing devices, a novel electrodynamic suspension (EDS) device—based on a semicircular track and cylindrical permanent magnet (PM) Halbach array—is presented in this paper. It enables a vehicle to statically levitate above a semicircular track. In order to calculate the electromagnetic force created by this novel device, we first create a 2-D equivalent linear model of the cylindrical PM Halbach array, build differential equations (based on the linear model) for the magnetic vector potentials, and produce the expression of the electromagnetic force per unit length by solving the equation system. Next, by integrating the electromagnetic force per unit length with the arc direction of the inner semicircular track, the vertical electromagnetic force created by the novel device can be determined. Analytic expression results, and those of a finite element analysis (FEA) model built by Maxwell are compared, and show the average relative error to be 3.02%. The novel device is rational, and the analytic expression is accurate.

Index Terms ─ Analytical calculation, cylindrical PM Halbach array, EDS, electromagnetic force, static levitation.

I. INTRODUCTION

The translational motion of a PM above a conductive plate simultaneously creates an electrodynamic levitation force. Because EDS systems are simple, reliable, and stable, they have become a popular research topic in the Maglev field. Magplane is the most common example of this system [1,2]. At low speeds, drag force dominates and results in a small levitation force insufficient for vehicle suspension [3-5]. In order to overcome the deficiencies of existing devices, various topologies—using coils or conductive plates—have been proposed to minimize drag force and maximize levitation force. Lawrence Livermore National Laboratory proposed an Inductrack suspension system [6], in which a coil was placed below a PM array. Kratz and Chen studied a null-current EDS system [7,8] with a double PM Halbach array and conductive plate. Musolino numerically studied a null-flux system with PMs, a cylindrical conductive sheet, and null-flux coil [9]. These topologies all share the characteristic of reduced drag force, but the vehicle cannot be suspended in stationary and low-speed states. Bird studied an electrodynamic wheel [10,11] able to suspended a vehicle at any speed state. However, structural constraints of the PM wheel and track result in a limited levitation force that is only applicable to small devices. A novel electrodynamic suspension device is proposed in this paper. The device, shown in Fig. 1, is able to produce a large electromagnetic force at any vehicle state. Meanwhile, calculating electromagnetic force created by this device.

Numerical computation results are usually accurate [12-14], but fail to reflect the inherent relationships among different parameters. Alternatively, analytical calculations herein consist of a 2-D and 3-D model, Chen studied a null-flux topology using the 3-D model [15], while Cho derived the 2-D force equations for a single Halbach PM array moving above a conductive plate [4]. The advantage of the latter is also useful for 2-D modeling because it enables the magnetic field and force to be neatly formulated with respect to the conducting boundary [16].

The objective of this paper is to analytically derive

Submitted On: April 28, 2016
Accepted On: October 19, 2018

the general 2-D force that can be immediately used to compute the force due to eddy currents that is rotating above a semicircular track.

II. PROPOSED SYSTEM

The proposed configuration employs the same PM arrangement on each of the two guide-ways, as shown in Fig. 1. The 3-D and 2-D schematic of this cylindrical EDS system are shown in Fig. 2 and Fig. 3.

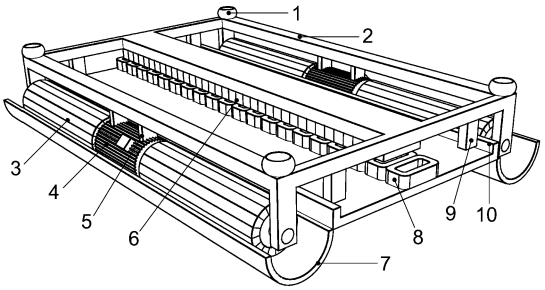

Fig. 1. Configuration of the cylindrical EDS device. 1: air spring, 2: chassis assembly, 3: PM Halbach rotor, 4: rotating motor with double extensions, 5: fixed module for motor, 6: propulsion magnets, 7: semicircular track, 8: LSM windings, 9: supporting block for location, and 10: limit baffle plate.

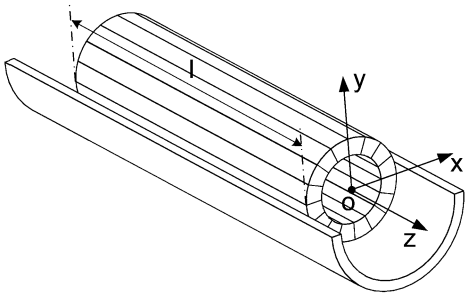

Fig. 2. 3-D schematic of the cylindrical EDS system.

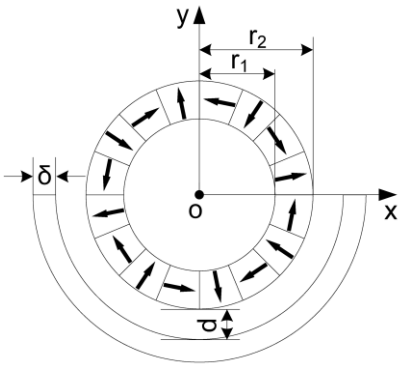

Fig. 3. 2-D schematic of the cylindrical EDS system.

In a maglev frame, four cylindrical PM modules are in pairs and symmetrically arranged in the track along the left and right sides. On each side, two modules are installed on the output shafts of the rotating motor with double extensions. While the maglev vehicle operates in the static state, the geometric center of the output shaft, cylindrical PM module, and semicircular guide groove are coincided in a side. The two rotating motors, which are fixed on both sides of the suspension frame and rotate in opposite directions at the same speed, drive the PM Halbach rotors. Relative movement between the PM rotors and the guide rail creates an eddy current in the rail, thereby generating the electromagnetic force. The resultant force is shown as only the vertical levitation force when there is no lateral movement. Otherwise, it includes the lateral guiding force.

III. EQUIVALENT MODEL

In Fig. 4, the unit arc length sheet, by means of symbol Δs, obtains the electromagnetic force F_0 of the PM rotor. The *x* and *y* components of this force are the guiding force F_{x0} and levitation force F_{y0}, respectively. By integrating the electromagnetic force, F_0, with the arc direction of the semicircular track, the vertical levitation force created by the cylindrical PM array can be determined. Where F_0 is the vertical electromagnetic force in the equivalent linear model as shown in Fig. 5. Without regard to lateral movement, the resultant force F_{x0} is zero as a consequence. We only discuss the approximate analytical expression of the vertical electromagnetic force in this paper.

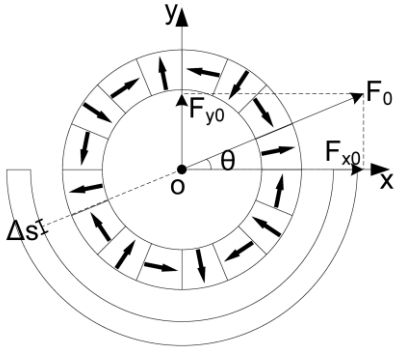

Fig. 4. 2-D cylindrical EDS model and its forces.

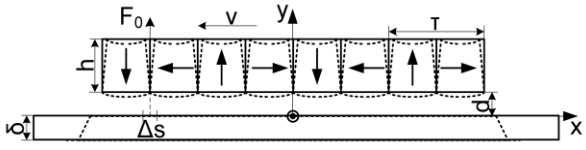

Fig. 5. The 2-D equivalent model.

IV. GOVERNING EQUATIONS

The 2-D equivalent linear model for the analytical solution is shown in Fig. 6. The axial length of the semicircular track is assumed to be sufficient, while the track itself is assumed to have constant conductivity, be nonmagnetic, and simply connected.

A. Conductive region, Ω_{II}

The surface density of an eddy current induced in a conductive plate by a moving source can be expressed as:

$$\boldsymbol{J} = \sigma \boldsymbol{E}, \tag{1}$$

$$\boldsymbol{E} = \boldsymbol{v} \times \boldsymbol{B}, \tag{2}$$

where $\boldsymbol{J}$ = surface density of the eddy current, σ = conductivity, $\boldsymbol{E}$ = electric field intensity, $\boldsymbol{v}$ = velocity vector, and $\boldsymbol{B}$ = magnetic flux density. Additionally, it is represented by the scalar equation:

$$J = -\sigma v B_y^s. \tag{3}$$

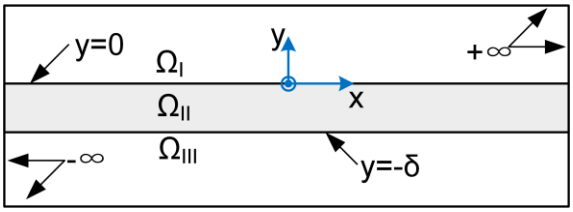

Fig. 6. Illustrating the conductive and nonconductive regions and boundaries.

Based on Ampère's circuital law and fundamental equation,

$$\nabla \times \boldsymbol{H} = \boldsymbol{J} + (\sigma + j\omega\varepsilon)\boldsymbol{E}, \tag{4}$$

$$\boldsymbol{B} = \nabla \times \boldsymbol{A}, \tag{5}$$

$$-\nabla\varphi = \boldsymbol{E} + j\omega\boldsymbol{A}, \tag{6}$$

$$\boldsymbol{B} = \mu_0 \boldsymbol{H}, \tag{7}$$

where $\boldsymbol{H}$ = magnetic field strength, ω = source frequency, ε = permittivity of the conductive plate, $\boldsymbol{A}$ = magnetic vector potential, φ = electric potential, and μ_0 = permeability of the conductive plate. Substituting (5), (6), and (7) into (4) and rearranging leads to:

$$\nabla^2 \boldsymbol{A} + k^2 \boldsymbol{A} = -\mu \boldsymbol{J} + \nabla\left(\nabla \cdot \boldsymbol{A} - \frac{k^2}{j\omega}\varphi\right), \tag{8}$$

and

$$k^2 = -j\omega\mu(\sigma + j\omega\varepsilon), \tag{9}$$

where k is a propagation function, using the Lorenz gauge,

$$\nabla \cdot \boldsymbol{A} - \frac{k^2}{j\omega}\varphi = 0. \tag{10}$$

The magnetic vector potential equation is:

$$\nabla^2 \boldsymbol{A} + k^2 \boldsymbol{A} = -\mu \boldsymbol{J}, \tag{11}$$

and in the 2-D model—as the magnetic vector potential, $\boldsymbol{A}$, only has a z component—is:

$$\nabla^2 A_z^{II} + k^2 A_z^{II} = -\mu J, \text{ in } \Omega_{II}. \tag{12}$$

B. Nonconductive regions, Ω_I, Ω_{III}

Because $\boldsymbol{J}$=0 in the nonconductive regions Ω_I and Ω_{III}, (11) simplifies to:

$$\nabla^2 A_z^{I} + k^2 A_z^{I} = 0, \text{ in } \Omega_I, \tag{13}$$

$$\nabla^2 A_z^{III} + k^2 A_z^{III} = 0, \text{ in } \Omega_{III}. \tag{14}$$

C. Boundary conditions

The conducting boundary conditions for the tangential field on the conductive plate surfaces are:

$$H_x^{I} - H_x^{II} = 0, \text{ at } y = 0, \tag{15}$$

$$H_x^{II} - H_x^{III} = 0, \text{ at } y = -\delta. \tag{16}$$

Based on the relationship between magnetic field strength and magnetic vector potential,

$$H_x = -\frac{1}{\mu}\frac{\partial A_z}{\partial y}. \tag{17}$$

Using (17) in (15) and (16) may lead to:

$$-\frac{\partial A_z^{I}}{\partial y} - \left(-\frac{\partial A_z^{II}}{\partial y}\right) = 0, \text{ at } y = 0, \tag{18}$$

and

$$-\frac{\partial A_z^{II}}{\partial y} - \left(-\frac{\partial A_z^{III}}{\partial y}\right) = 0, \text{ at } y = -\delta. \tag{19}$$

The inner boundary conditions of the joint face on the conductive plate surfaces are:

$$A_z^{I} = A_z^{II}, \text{ at } y = 0, \tag{20}$$

and

$$A_z^{II} = A_z^{III}, \text{ at } y = -\delta. \tag{21}$$

Additionally, the outer non-conducting boundary conditions are:

$$\lim_{y \to +\infty} A_z^{I} = 0, \tag{22}$$

and

$$\lim_{y \to -\infty} A_z^{III} = 0. \tag{23}$$

D. Source field

In the 2-D equivalent linear model, space magnetic field due to a PM Halbach array can be expressed as [17,18]:

$$B_x^s = B_0 e^{-p(-y+d)} e^{j(px-\pi/2)}, \tag{24}$$

and

$$B_y^s = B_0 e^{-p(-y+d)} e^{jpx}, \tag{25}$$

where

$$B_0 = [B_r(1 - e^{-ph})\sin\frac{\pi}{m}] / (\frac{\pi}{m}), \tag{26}$$

and B_x^s = magnetic flux density of the source field x-component, B_y^s = magnetic flux density of the source field y-component, B_r = magnet remanence, m is the

number of magnets in one pole-pair, and $p = \pi / \tau$ (where τ = pole pitch).

V. GENERAL SOLUTION

Applying the separation of variables principal to (11)-(13), the solution within each region is [8, 18]:

$$A_z^{\mathrm{I}} = (C_1 e^{-R_1 y} + C_2 e^{R_1 y}) e^{jpx}, \tag{27}$$

$$A_z^{\mathrm{II}} = [C_3 e^{-R_2 y} + C_4 e^{R_2 y} + \phi(y)] e^{jpx}, \tag{28}$$

$$A_z^{\mathrm{III}} = (C_5 e^{-R_3 y} + C_6 e^{R_3 y}) e^{jpx}, \tag{29}$$

where $R_i = \sqrt{p^2 - k_i^2}$, $\phi(y) = \dfrac{\mu_0 \sigma v B_0 e^{-p(-y+d)}}{k_2^2}$.

C_1-C_6 are unknowns that must be determined by means of boundary conditions (18)-(23). Therefore, the reflected field due to the induced current in the conducting plate may be expressed as:

$$B_x^r = -\frac{\partial A_z^{\mathrm{II}}}{\partial y}, \tag{30}$$

and

$$B_y^r = -\frac{\partial A_z^{\mathrm{II}}}{\partial x}. \tag{31}$$

When the translational motion of a PM is above the conductive plate, the total field is:

$$B_x = B_x^s + B_x^r, \tag{32}$$

$$B_y = B_y^s + B_y^r, \tag{33}$$

and the surface density of the eddy current is:

$$J_e = -\sigma v B_y. \tag{34}$$

VI. FORCE EQUATIONS

A. Electromagnetic force of an equivalent linear model

The vertical electromagnetic forces per unit width and length evaluated along the top of the plate surface is:

$$F_0 = -\frac{1}{2} \mathrm{Re} \int_{-\delta}^{0} J_e B_x^* dy, \tag{35}$$

where B_x^* is the complex conjugate of the magnetic field x-component.

B. Electromagnetic force of a 2-D cylindrical model

In order to calculate the electromagnetic force of the 2-D cylindrical model, it did this integral by along the arc direction in inboard semicircular track shown in Fig. 4. When $\Delta s \to 0$, $ds = R \cdot d\theta$, where R = the inside radius of the semicircular track. The levitation force of the Halbach rotor can be expressed as:

$$\begin{aligned} F_y &= \int_0^{\pi R} F_0 \sin\theta ds = \int_0^{\pi} F_0 R \sin\theta d\theta \\ &= -\frac{1}{2} \mathrm{Re} \int_0^{\pi} \int_{-\delta}^{0} J_e B_x^* R \sin\theta dy d\theta \end{aligned}. \tag{36}$$

VII. MODEL VALIDATION

The 2-D equivalent linear modeling approach was validated by creating an equivalent radial electromagnetic force for a PM Halbach rotor using a finite element analysis (FEA) model.

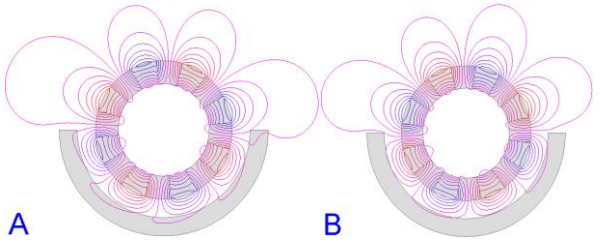

Fig. 7. PM Halbach rotor magnetic field transient simulation contour—plot at 360 rpm (shown in A) and 1620 rpm (shown in B).

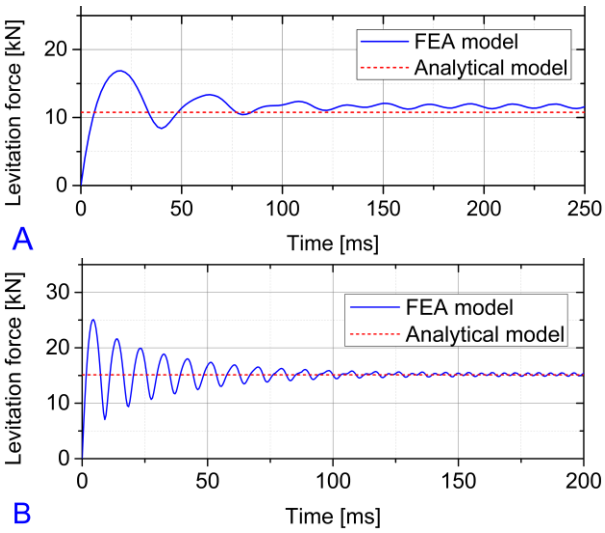

Fig. 8. 2-D transient results for the four pole-pair Halbach rotor at 360 rpm (shown in A) and 1620 rpm (shown in B).

Figure 7 shows the Halbach rotor magnetic field transient vector potential contour—plot at one timestep. Figure 8 shows the levitation force for rotating speeds of 360 rpm and 1620 rpm. The simulation parameters are shown in Table 1.

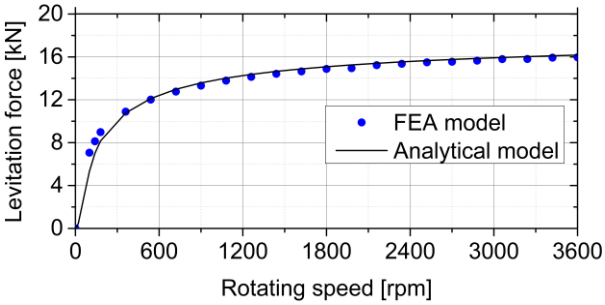

Fig. 9. The levitation force at different rotating speeds.

Figure 9 compares the analytic expression results with those of the finite element method built by Maxwell business software. They describe different rotational speeds with the parameters shown in Table 1. Figure 10 shows that the average relative error is 3.02%.

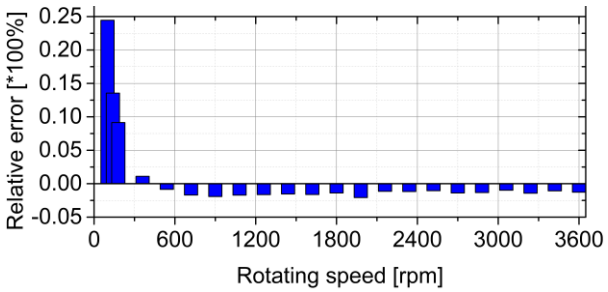

Fig. 10. Levitation force relative error as a function of rotating speed.

Table 1: Simulation parameters

Description		**Value**
Magnet	Number of pole-pairs, p	4
	Remanence, B_r	1.18 T
	Relative permeability, μ_r	1.067
	Outer radius, r_2	150 mm
	Inner radius, r_1	100 mm
	The axial length of a single magnet, l	1000 mm
Track	Conductivity, σ	3.8×10^7 S/m
	Outer radius, r_4	230 mm
	Inner radius, r_3	190 mm
	The thickness of track, δ	40 mm
	The length of a track, l_t	1000 mm
Air Gap	The vertical air gap between rotor and track, d	40 mm

VIII. DISCUSSION

From Fig. 9, the levitation force increases gradually and tends to saturation at 0-3600 rpm. Additionally, the nonmagnetic metal track can be used as an anti-magnet to concentrate magnetic field lines at higher rotor rotation speeds, as shown in Fig. 7.

The vertical magnetic force enables the vehicle to statically levitate above the semicircular track. Hence, the levitation force is analyzed for the different vertical air gap occurring at w = 720 rpm, 1620 rpm, and 3060 rpm. The vertical levitation stiffness was investigated in the same run. The steady vertical motion was interrupted every millimeter when the vertical air gap was between 20 and 50 millimeters. The result of such levitation force is shown in Fig. 11. The slope of the points on the levitation force curve gives the magnitude of the vertical stiffness. We plot the obtained stiffness coefficient as a function of the vertical air gap to show how the stiffness increases rapidly as the gap is reduced, as shown in Fig. 12.

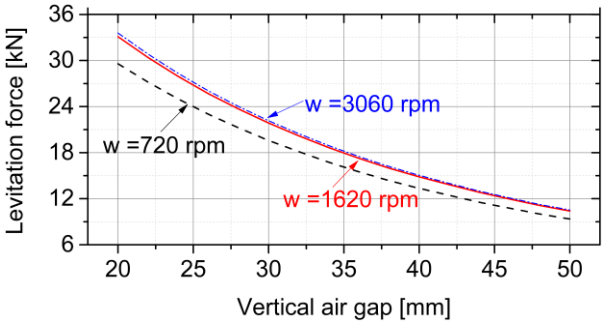

Fig. 11. The electromagnetic force and vertical air gap, when w =720 rpm, 1620 rpm, and 3060 rpm.

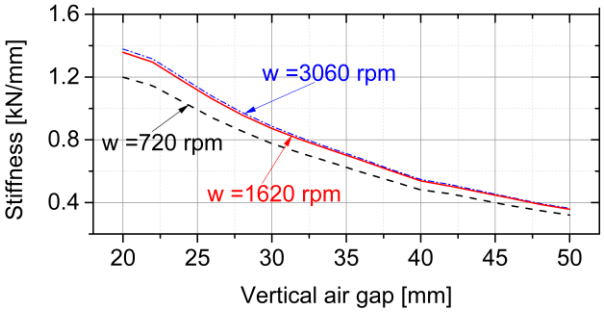

Fig. 12. Stiffness coefficient and vertical air gap when w =720 rpm, 1620 rpm, and 3060 rpm.

Using the structure parameters shown in Table 1 of the cylindrical PM electrodynamic suspension vehicle, a single cylindrical PM module can create a levitation force of 15000N at a rotating speed of 1620 rpm—calculated by the analytic and FEA method.

However, there is some limitation in our model. Unlike other electrodynamic systems that use the conductor plate and Halbach PMs, in this model, the magnetic field on the semicircular guide groove has a periodicity change, thus causing periodic, small-range fluctuations to the levitation force.

IX. CONCLUSION

A cylindrical PM EDS device that enables a vehicle to statically levitate above a semicircular track has been presented. A 2-D equivalent analytic calculation method has been deduced through second order vector potential and integral analysis. The method models the forces created when a Halbach rotor is rotating and moving above a semicircular, nonmagnetic metal guideway. The analytic model was validated by the finite element method.

ACKNOWLEDGMENT

This article was supported by the Key Laboratory Project of the Ministry of Education (No. 2682013ZT18). The authors would like to thank the Ansys Corporations for the use of their finite element analysis software, Maxwell.

REFERENCES

[1] J. Fang, A. Radovinsky, and D. B. Montgomery, "Dynamic modeling and control of the magplane vehicle," *Proceedings of The 18th International Conference on Magnetically Levitated Systems and Linear Drives*, Maglev'2004, China, Oct. 2004.

[2] D. B. Montgomery, "Overview of the 2004 magplane design," *Proceedings of The 18th International Conference on Magnetically Levitated Systems and Linear Drives*, Maglev'2004, China, Oct. 2004.

[3] H. Hieronymus, J. Miericke, F. Pawlitschek, and M. Rudel, "Experimental study of magnetic forces on normal and null flux coil arrangements in the inductive levitation system," *Applied Physics*, vol. 3, no. 9, pp. 359-366, 1974.

[4] H. Cho, H. Han, J. Bang, H. Sung, and B. Kim, "Characteristic analysis of electrodynamic suspension device with permanent magnet Halbach array," *J. Appl. Phys.*, vol. 105, 2009.

[5] H. Cho, D. K. Bae, H. Sung, and J. Lee, "Experimental study on the electrodynamic suspension system with HTSC and PM Halbach array magnets," *IEEE Trans. Appl. Superconduct.*, vol. 18, no. 2, pp. 808-811, 2008.

[6] R. F. Post and D. D. Dyutov, "The Inductrack: A simpler approach to magnetic levitation," *IEEE Trans. Appl. Superconduct.*, vol. 10, no. 1, pp. 901-904, 2000.

[7] R. Kratz and R. F. Post, "A-current electrodynamic levitation system," *IEEE Trans. Appl. Superconduct.*, vol. 12, no. 1, pp. 930-932, 2002.

[8] Y. Chen and K. Zhang, "Electromagnetic force calculation of conductor plate double Halbach permanent magnet electrodynamic suspension," *ACES Journal*, vol. 29, no. 11, pp. 916-922, 2014.

[9] A. Musolino, M. Raugi, R. Rizzo, and E. Tripodi, "Stabilization of a permanent-magnet Maglev system via null-flux coils," *IEEE Trans. on Plasma Sci.*, vol. 43, no. 5, pp. 1242-1247, 2015.

[10] J. Z. Bird and T. A. Lipo, "Modeling the 3-D rotational and translational motion of a Halbach rotor above a split-sheet guideway," *IEEE Trans. Magn.*, vol. 45, no. 9, pp. 3233-3242, 2009.

[11] J. Z. Bird and T. A. Lipo, "Calculating the forces created by an electrodynamic wheel using a 2-D steady-state finite-element method," *IEEE Trans. Magn.*, vol. 44, no. 3, pp. 365-372, 2008.

[12] P. Zheng, B. Yu, H. Yan, Y. Sui, J. Bai, and P. Wang, "Electromagnetic analysis of a novel cylindrical transverse-flux permanent-magnet linear machine," *ACES Journal*, vol. 28, no. 9, pp. 878-890, 2013.

[13] H. Rezaei and S. V. Zadeh, "Modelling and analysis of permanent electrodynamic suspension systems," *Prog. Electromagn. Res. M*, vol. 36, pp. 77-84, 2014.

[14] A. N. Khodabakhsh, S. V. Zadeh, and A. H. Isfahani, "Finite element analysis and experimental implementation of the cylindrical permanent magnet electrodynamic suspension system," *Electromagnetics*, vol. 29, no. 7, pp. 563-574, 2009.

[15] Y. Chen, W. Zhang, J. Z. Bird, S. Paul, and K. Zhang, "A 3-D analytic-based model of a null-flux Halbach array electrodynamic suspension device," *IEEE Trans. Magn.*, vol. 51, no. 11, article# 8300405, 2015.

[16] N. Paudel and J. Z. Bird, "General 2-D steady-state force and power equations for a traveling time-varying magnetic source above a conductive plate," *IEEE Trans. Magn.*, vol. 48, no. 1, pp. 95-100, 2011.

[17] J. F. Hoburg, "Modeling maglev passenger compartment static magnetic field from linear halbach permanent magnet arrays," *IEEE Trans. Magn.*, vol. 40, no. 1, pp. 59-64, 2004.

[18] Y. Chen, "Characteristic Analysis of Low Speed Electrodynamic Suspension," *Ph.D. Dissertation*, Department of Electrical Engineering, Southwest Jiaotong University, Chengdu, China, 2015.